

Structural entanglements in protein complexes

Yani Zhao, Mateusz Chwastyk, and Marek Cieplak*

Institute of Physics, Polish Academy of Sciences, Aleja Lotników 32/46, PL-02668 Warsaw, Poland

We consider multi-chain protein native structures and propose a criterion that determines whether two chains in the system are entangled or not. The criterion is based on the behavior observed by pulling at both termini of each chain simultaneously in the two chains. We have identified about 900 entangled systems in the Protein Data Bank and provided a more detailed analysis for several of them. We argue that entanglement enhances the thermodynamic stability of the system but it may have other functions: burying the hydrophobic residues at the interface, and increasing the DNA or RNA binding area. We also study the folding and stretching properties of the knotted dimeric proteins MJ0366, YibK and bacteriophytochrome. These proteins have been studied theoretically in their monomeric versions so far. The dimers are seen to separate on stretching through the tensile mechanism and the characteristic unraveling force depends on the pulling direction.

I. INTRODUCTION

There is a growing interest in proteins that contain knots¹⁻³. Chronologically, the first entry on the list of such proteins appears to be carbonic anhydrase B^{4,5} and the current status of the list can be obtained, for instance, at the KnotProt database⁶. The protein backbones do not form closed loops, however, and the presence of a knot cannot be assessed in absolute terms as it depends on the method used to connect the termini beyond the backbone in order to generate a closed line. A common computational approach to determine the location of a knot is to use the KMT algorithm^{7,8} which reduces the topological complexity of the backbone in a step-wise fashion by decreasing the number of segments. The reduced structure brings out the topology and allows for a determination of the sequential locations of the knot's ends. It should be noted that this approach does not impose any closure of the backbone line which may sometimes result in not detecting a knot that appears to be present. The KMT algorithm leads to an observation that carbonic anhydrase B contains a shallow knot, since one of the knot ends is just three sites away from the C-terminus. Topologically, it is very easy to untie it and then tie it back. On the other hand, for deeply knotted proteins, both ends of the knot are at a substantial distance away from the termini and tying such a knot is much harder. An experimental way to tell the existence of the knot is to stretch a monomeric protein by the terminal sites⁹⁻¹². The knot is thought to be present if the utmost backbone extension is noticeably shorter than the contour length, as the tightened knot takes away a portion of the chain that could be extended.

In this paper, we consider multi-chain protein complexes and focus on the entanglement effects that arise from interactions between separate unknotted chains. In some complexes, the individual chains may themselves be entangled when they contain knots. In fact, many of the well studied knotted proteins, such as the deeply knotted YibK methyltransferase from *Haemophilus influenzae* (PDB:1J85)^{13,14} and the shallowly knotted MJ0366 from methanogenic archaea *Methanocaldococcus jannaschi* (PDB:2EFV) are actually dimeric. In these systems, the native entanglement is found in each of the chains individually and, in principle, can be attested experimentally through stretching of single chains. However, such single-chain stretching does not test the entanglements that arise from interactions between two chains (knotted or unknotted). We propose that the way to detect them is by pulling at four termini instead of two. If the termini of one chain are denoted by N and C, and of the other by N' and C', then we propose to pull by N-C and, simultaneously, by N'-C'. Alternatively, we can anchor N and C while pulling simultaneously by N'-C' along the line connecting N' with C'. The two chains are considered to be unentangled if this action results in separation of the chains. Otherwise, we declare the chains to be entangled. Sometimes, anchoring N' and C' combined with pulling by N and C may result in a different verdict. We refer to such situations as type-I entanglement in distinction to type-II entanglement which is unambiguous. We discuss this point later.

It should be noted that the four-terminal pulling process of two chains is quite distinct from the two-terminal stretching of a dimer. In the former case, pulling takes place in each of the chains and the termini of each chain are pulled along the same direction. In the latter case, two termini are anchored and stretching takes place either in one chain or it works to separate one chain from another in a variety of possible ways. The chosen termini are then stretched in opposite directions. In a dimer, there are six choices to pick two termini out of four: N-C, N'-C', N-C', N'-C, C-C', and N-N'. Stretching is assumed to take place along the line connecting the selected termini. The outcomes of the two-terminal processes usually depend on this choice, as demonstrated in the context of unknotted proteins¹⁵⁻¹⁸: the chains may or may not separate on stretching and the characteristic unravelling forces are anisotropic. In the examples of knotted dimers considered here, the two chains are connected by a number of contacts but are not mutually entangled. In these situations, the dynamics of the N-C stretching is found to be affected by the

presence of the other chain only in a minor way, but the cross-chain stretchings are very distinct.

Here, we report on many instances of inter-chain entanglement found in our survey of 10 498 n -meric protein structures, where $n \geq 2$. The structures, both homomeric and heteromeric, were obtained from the Protein Data Bank (PDB), in an essentially random way, by considering all 4-character alphanumerical structure codes in which the two middle characters are between "00" and "cz". About 900 of these, i.e. 8.6%, were found to be entangled. In addition, we also consider six large ribosomal complexes, corresponding to the PDB codes of 3JCT, 4V4J, 5FCJ, 5IT7, 5J88, and 5J86. We analyze a number of examples of the resulting cases of entanglement in detail. Our four-terminal pulling is implemented by using a structure-based coarse-grained model^{19–22}. Any other molecular dynamics approach is expected to lead to similar conclusions regarding the detection of entanglement. However, the dynamics of the pulling process itself should depend on the model and the pulling speed. As to the function of the interchain entanglement, it is possible that it leads to an increased thermal stability of the system.

Experiments on knotted proteins have been done for monomeric systems such as ubiquitin hydrolases UCH-L1 (PDB:2ETL)²³ and UCH-L3 (PDB:1XD1)²⁴ or a bacteriophytochrome (PDB:2O9C)⁹, even though the latter protein forms dimers in a solution. (From now on, we shall refer to the proteins by their PDB structure codes for brevity.) Another purpose of this paper is to reconsider the folding and stretching properties of the knotted 1J85, 2EFV, and 2O9C proteins by noticing the fact that they function as dimers that are bound by hydrogen and hydrophobic bonds. Unlike most of the cysteine-knot dimers¹⁶, there are no covalent bonds between the chains. So far, theoretical studies of these systems have been restricted to monomers. Monomeric models of 1J85 have been considered, for instance, in refs.^{10,12,25,26} and of 2EFV in refs.^{27–29}. One of the results obtained was that the probability to form a knot on folding is enhanced by on-ribosome folding^{26,29}. Here, however, we do not consider folding under nascent conditions. The three knotted dimers considered here are not entangled when using the 4-termini pulling test – the chains just separate.

It should be noted that entanglements are known to arise and disappear spontaneously in dense polymeric liquids^{30,31}, whereas the topological effects discussed here appear in the native state of several polypeptide chains. Such chains have been considered recently by Baiesi et al.³². Specifically, they have identified 110 domain-swapped dimers^{33,34} and determined their linking numbers³⁵. These numbers, denoted here as L_k , are obtained by closing the chains into loops and then evaluating the Gauss double linking integrals. The L_k indicates the number of times that one closed curve winds around another in the three-dimensional space. Generally, a pair of chains is entangled if the absolute value of L_k is larger than 0 (one exception is the Whitehead link).

The protein systems we study need not involve domain swapping and need not have sequentially identical chains. Most of them (over 85%) are not domain-swapped but only a few are sequentially heterogeneous. The list of the protein studied is shown in Table SI in the Supplementary Material (SM).

II. STRUCTURE-BASED MODELING

We use a Go-like model³⁶ with the specific implementation as described in refs.^{20–22}. The length-related parameters in the bonding and non-bonding potentials are derived from the native structure. The molecular dynamics employed here deals only with the α -C atoms and the solvent is implicit. The bonded interactions are described by the harmonic potentials. Non-bonded interactions, or contacts, are assigned to pairs of amino acids by using the overlap criterion in which the heavy atoms in the native conformation are represented by enlarged van der Waals spheres^{20,37,38}. The contact exists if at least two such spheres from different residues overlap. These contacts are described by the Lennard-Jones potentials with the minima at the crystallographically determined distances. The contact potentials have a depth, ϵ , which is identical in each contact. Non-native contacts are considered repulsive. Variants with non-uniform values of ϵ have been shown²¹ to yield statistically similar behavior in a test set of 28 proteins.

The backbone stiffness is accounted for by the chirality potential²⁰ which favors the native sense of the local backbone chirality. The value of ϵ has been calibrated by making comparisons to the experimental data on stretching: approximately, $\epsilon/\text{\AA}$ is 110 pN (which also is close to the energy of the O-H-N hydrogen bond of 1.65 kcal/mol and close to 1.5 kcal/mol derived as a typical value in loop parts of a protein through all-atom simulations³⁹). For most unknotted proteins, optimal folding takes place around the temperature, T , of $0.3 \epsilon/k_B$ (k_B is the Boltzmann constant; the stiffness parameters depend on ϵ) and this temperature should correspond to a vicinity of the room T .

We use the Langevin thermostat with substantial damping. The time unit of the simulations, τ , is effectively of order 1 ns as the displacement of the atoms is dominated by diffusion instead of ballistic motions. Folding is declared as accomplished when all native contacts are established for the first time (the distance between two α -C in a contact is smaller than the native distance

multiplied by 1.5). For knotted proteins, however, this condition does not necessarily signify formation of the native knot. The situation in which there is no knot but all contacts are established is referred to as misfolding. It should be noted that the contacts can be set and then broken multiply due to the thermal fluctuations.

When studying folding, we prepare the starting state of a dimeric protein by heating the native structure to $T = 1.5 \epsilon/k_B$ and make sure that all of its native contacts are broken. Each folding trajectory, at a much lower T , starts from a different conformation. Proper folding is declared to take place if all native contacts are established and so are the knots. The simulations are performed in an infinite space so some of the trajectories may result in the two chains never meeting again. Similar strategy is used to fold 2O9C monomers because of its covalently bound ligand. In the holoprotein form (a conjugated protein contains a cofactor), this ligand is not cleaved off from the initial conformation during folding to prevent the situation that it fluctuates too much to make a contact with the protein. In case when the ligand is reduced, one obtains the apoprotein of 2O9C. In the coarse-grained model, we represent the ligand of 2O9C by 20 effective atoms located at the backbone carbon atoms⁴⁰.

Pulling is accomplished at a constant speed, v_p , along the direction that connects two termini in the native state. It has to be noted that, this choice of the direction is just one of many and the outcome of the procedure generally depends on it (see Fig. S1 in SM). When determining the existence of an entanglement, we use v_p of $0.01 \text{ \AA}/\tau$. The choice of the value of v_p may affect the dynamics of the testing process but has no relevance for the outcome regarding the overall topology. The termini involved in pulling are attached to harmonic springs of elastic constant $k = 0.12 \epsilon/\text{Å}$, which is close to the values corresponding to the elasticity of cantilevers in atomic force microscopes. For a given multi-chain protein, we consider all possible pair permutations. The chains are considered to be separated if the centers of mass of the chains are further away from each other than the contour length of one chain. Entanglement shows as a rapid growth in the resisting force and we stop the test if the force exceeds $25 \epsilon/\text{Å}$. When studying the very process of stretching, we take v_p of $0.005 \text{ \AA}/\tau$, which is some 2 orders of magnitudes faster than typical experimental speeds.

III. INTERCHAIN ENTANGLEMENTS

The self-association of proteins resulting in the formation of multimers is a common phenomenon in nature. For example, only a third of human enzymes are monomers, the rest are multimers⁴¹. In bacteria (*Escherichia coli*), about 19.4% of proteins are monomeric and 38.2% dimeric, the other are multimers composed of more than 2 monomers⁴². Usually, the self-association takes place either through the 3-dimensional domain swapping (molecular exchanges of structural elements in one chain with the corresponding parts of another) or by various two-residue interactions including hydrophobic, chemical cross-linking, and electrostatic that do not pertain to the full domains⁴³. Out of about 900 cases of entanglement identified by us, most are shallowly entangled in which the entanglement disappears if one cuts away at most 10 residues from one or both termini. Otherwise, the chains are considered to be entangled deeply. We classify these entanglements into two types. In type I, the presence of the entanglement depends on the pulling direction. For example, the electron transport protein PDB:5AUR, shown in Fig. 1, is considered entangled if one anchors N' and C' in one chain (chain C shown in blue) and pulls by N and C in another (chain A shown in red) away from the first chain. However, it becomes disentangled if one anchors N and C and pulls away N' and C'. The entanglement is considered to be of type II if its presence does not depend on the pulling direction of the chains. In Fig. 2, the top two examples are of type I and the bottom two of type II.

The types of the entanglement are related to L_k . Type I is associated with L_k of 1 or -1. Type II requires that the absolute value of L_k must be larger than 1 (as in the case of 1C1G), or that it switches between 1 and 2 depending on how one closes the open protein chains into loops. One example of the latter situation is 4AAI (see Fig. S1 in SM), in which one chain winds around the other more than once but less than twice. If one selects the pulling direction statistically (for example by randomly sampling the angle with respect to the line that connects the termini), the average value of $|L_k|$ of type I would be between 0 and 1, because for each choice it can be only equal to either 1 or 0 ($L_k = 0$ if there is no entanglement). For type II entanglement, $|L_k|$ is larger than 1 on average. Actually, the closure of the chains is decided by the pulling direction in our model, because L_k is best estimated after the chains are fully pulled. As shown in the right panels of Fig. 2, the closure of fully pulled chains is very straightforward – we connect N with C and N' with C' by straight lines and does not need any ensemble of possible closures as done in ref.³². We point out that the role of L_k here is not to detect the entanglement, as this is accomplished by pulling, but to determine the entanglement type. We can conclude that L_k depends on the pulling direction of chains and much less so on the specifics of the closure.

For a more detailed discussion, we have selected 15 deeply entangled chains. They are listed in Table I together with some structural information. Their native and pulled conformations are shown in Fig. 2 and in Figs. S2 and S3 in SM. The remaining examples are listed in Table SI in SM. Among the 15 cases, 1A73, 1AV1, 4ANG, 2A68, 2A8C, 4A9Z, 5AUR, and 5FCJ are

endowed with entanglement of type I whereas 1C1G, 2ADL, 1C4D, 2AHR, 3A1M, 3AQJ and 4AAI of type II.

The self-association of chains is expected to increase the thermal stability of the combined system. We demonstrate it here for protein 4AAI (E73). Its two sequentially identical chains form a large cavity on the surface of the protein. This cavity is distal to the canonical DNA binding site and it is positively charged. It also forms a potential ligand binding site⁴⁵. Fig. 3 (top panel) shows the entangled native structure of 4AAI on the left and its twisted untangled version on the right. The twisted structure is prepared by using the sculpting tool of the PyMol package⁴⁶. As a result of the twist, the intrachain contacts remain the same but the number of the interfacial contacts is reduced by 19 (the total number of contacts in the native structure is 328). Fig. 4 (top panel) shows that the twist results in larger RMSF equilibrium fluctuations in almost the entire chain and the downward shift by about $0.017 \epsilon/k_B$, (i.e. by about 14 K) in the melting temperature T_0 defined as a T at which the equilibrium-calculated P_0 crosses $\frac{1}{2}$. P_0 is defined as the probability that all native contacts are present simultaneously – for a discussion of this concept see ref⁴⁷.

Another example of a situation in which the role of the entanglement can be assessed is the 3-chain protein 3AQJ (the bacteriophage P2 tail spike protein)⁴⁸. The chains of 3AQJ wind around a threefold symmetry axis to form a triangular pyramid and the interior of the pyramid is occupied by hydrophobic side chains that provide stabilization. Here, we consider the entanglement of chains A and B that have L_k of 3. In this case, the entanglement can be removed by cutting the backbone at the three sites indicated in the bottom panels of Fig. 3 and then reconnecting on the other side of the intersection by using the PyMol package. As a result of this procedure, the number of the interfacial contacts in the reconnected structure is increased by 19 because the chains get closer together. This is opposite to the effect of twisting applied to 4AAI. At the same time, the intrachain contacts remain the same (there are 387 native contacts in the original native structure). These additional contacts slightly increase T_0 from 0.137 to 0.141 ϵ/k_B . Despite the bigger number of the interchain contacts, the reconnected structure is less stable when assessed based on the values of RMSF obtained at $T = 0.3 \epsilon/k_B$ (the left bottom panel of Fig. 3). The RMSF for the reconnected structure is larger than for the native structure at almost all sites. Notice that P_0 is a measure of how many native contacts are present independent of what is the actual distance between the corresponding α -C atoms, as long as the distance is below a threshold, whereas RMSF is a measure of the positional fluctuations. Thus the RMSF is a better characteristic of the structural stability in this context and we conclude that the entanglement indeed enhances the stability.

The entanglement of chains enhances the thermal stability, but is also expected to affect the very functioning of the complexes. Here, we just list some examples of n -mers in which the role of the entanglement should be elucidated. The tetrameric 1AV1 (truncated human apolipoprotein A-I) forms an antiparallel four-helix bundle shaped into an elliptical ring that keeps the hydrophobic residues at the interface⁴⁹. The tube-like dimeric 1C4D (gramicidin) forms an ion channel, which facilitates transport of ions across the hydrophobic barrier of the phospholipid membranes⁵⁰. The dimeric 4ANG (PRR1 coat protein) enhances the exposed binding surface for the RNA⁵¹. The homodimeric 1A73 (homing endonuclease) promotes deformation of the homing-site DNA that facilitates cleavage across the minor groove of DNA⁵². The coiled coil dimeric 1C1G (tropomyosin) stabilizes association of actin with non-muscle cells⁵³. These dimers wrap around actin filaments and form a head-to-tail overlapping polymer. This structure allows for flexibility between the dimers and makes tropomyosin stay strain-free along the filament.

IV. FOLDING AND STRETCHING OF THE KNOTTED DIMERIC PROTEINS

We now consider the three homodimeric proteins 2EFV, 1J85, and 2O9C that have been mentioned in the Introduction. Their structures are shown in Fig. 5. Folding is considered as a function of T and is based on between 200 and 500 trajectories. Stretching is considered at $T = 0.3 \epsilon/k_B$ and is based on 50 trajectories that last for at least 200 000 τ to ensure achieving separation if it takes place. Stretching is performed at the speed v_p of 0.005 $\text{\AA}/\tau$.

A. 2EFV

The monomer of 2EFV comprises 87 residues but the atomic coordinates of the first five of them are not available in the structure file. The secondary structures of 2EFV consists of four helices (23-32, 41-49, 62-71, 74-86), two 3-10 helices (33-35, 72-73), and two β -strands (12-17, 54-59). The knot is of the trefoil type and its ends are located at sites 11 and 73. The sequential separation, Δn , between the knot ends is thus 63. On stretching, Δn goes down in stages to about 10 residues^{10,12}, similar to what one gets for the deeply knotted 1J85 which also contains the trefoil knot^{10,12}. For the monomeric 2EFV, it has been shown²⁹ that a) a denatured chain folds to the knotted and globular native state much easier than the deeply knotted monomers, b) the set of possible topological folding pathways is richer than the one considered in ref.²⁷ – in addition to trajectories with a single knot-loop there are also trajectories with two smaller knot-loops, c) there is a range of optimal T 's in which knotting is successful,

d) nascent conditions boost the peak success rate to fold from 76% to 81% and eliminate single-loop trajectories. The nascent conditions occur on the ribosome⁵⁴⁻⁵⁹. In the simplest description, we have modelled them as a chain growing, one residue at a time, from a repulsive plane²⁶.

The folding process of the dimeric 2EFV is studied at two temperatures $T = 0.3$ and $0.45 \text{ } \epsilon/k_B$ to explore the role of the temperature effects. Folding is decided based on "all" native contacts being established for the first time. There are several possible meanings of the word "all" here and specifically, we consider three situations: monomeric (native contacts in the monomer), dimeric (all native contacts in the dimer), and monomeric (native contacts of the monomer) but in a process in which the other monomer is present dynamically – we just do not monitor its contacts. This last case is denoted as 'chain A (B present)'. Our results are displayed in Table II. It shows the probability of successful knotted folding, S_f , the probability of misfolding, S_{mf} , (the native contacts are established but the knot is not made or the knot is different than the one in the native state, and the knotting probability S_k . S_k is determined independent of whether the native contacts are established and by including knots of non-native types, if any. The types of knots are determined visually. The table also shows the median folding time, t_f , as obtained through the determination of S_f , and median knotting time, t_k .

For the monomeric 2EFV, S_f at $T = 0.45 \text{ } \epsilon/k_B$ is much higher than at $T = 0.3 \text{ } \epsilon/k_B$, which agrees with the previous work²⁹ that $T = 0.45 \text{ } \epsilon/k_B$ is the optimal off-ribosome folding temperature for 2EFV. Moreover, S_f of chain A is significantly increased in the presence of chain B at $T = 0.3 \text{ } \epsilon/k_B$, while that at $T = 0.45 \text{ } \epsilon/k_B$ remains almost the same. The interfacial interactions between the monomers seem promoting the folding of single chains at the lower temperature. We also found that the folding pathway of monomeric 2EFV at $T = 0.3 \text{ } \epsilon/k_B$ is different than at $0.45 \text{ } \epsilon/k_B$ as evidenced by the values of t_f . At $T = 0.3 \text{ } \epsilon/k_B$, the native contacts are established about four times faster than the time needed to make the knot. However, the opposite takes place at $T = 0.45 \text{ } \epsilon/k_B$. Our data suggests that tying a knot is more difficult when the effect of the thermal fluctuations is weaker. It appears that formation of the knot at $T = 0.45 \text{ } \epsilon/k_B$ stabilizes the protein and facilitates the establishment of the contacts.

Folding of dimers is much harder compared to monomers. For example, S_f for the dimeric 2EFV is 3% and 6% at $T = 0.3$ or $0.45 \text{ } \epsilon/k_B$ respectively compared to 5% and 65% obtained in the monomeric case. The successful folding of a dimer requires the folding of its two monomers simultaneously. When one monomer is folded the other may still be fluctuating. We observe that in 33% trajectories at $T = 0.3 \text{ } \epsilon/k_B$ (or 34% at $T = 0.45 \text{ } \epsilon/k_B$), chains A and B are well separated at the end of the simulations – the interfacial contacts are not formed.

There are three possible pathways to fold a dimeric 2EFV starting from the fully unfolded conformation. In the first pathway, denoted as \mathbb{F}_1 , two monomers fold nearly simultaneously, which is followed by the establishment of the interfacial contacts. In the second pathway, \mathbb{F}_2 , one monomer folds first and then the interfacial contacts are established, which is followed by folding of the other monomer. In the third pathway, \mathbb{F}_3 , interfacial contacts are established the first, which is followed by a simultaneous folding of the monomers. The results on the probabilities and time scales corresponding to the three pathways are listed in Table III. Examples of the folding pathways at $T = 0.3 \text{ } \epsilon/k_B$ can be found in Fig. 6. The evolution patterns can be characterized by providing the average fractions of the established native contacts Q_A , Q_B and Q_{INT} in monomers A, B, and at the interface respectively. Symbol Q will denote the fraction of all native contacts that are established. The time-dependence of these parameters can be found in Fig. 7. For example in pathway \mathbb{F}_1 , Q_{INT} reaches 1 in a slower way than Q_A and Q_B , while the opposite holds true in pathway \mathbb{F}_3 .

The knotting mechanisms of monomers in the dimeric structure are analogous to those found for the monomeric 2EFV: they are of the two- and single-loop kind. In 81% trajectories at $T = 0.3 \text{ } \epsilon/k_B$, both monomers get tied via the two-loops mechanism. In the remaining trajectories, one monomer is tied via the two-loops mechanism and the other by the single-loop mechanism. For $T = 0.45 \text{ } \epsilon/k_B$, both monomers get tied via the two-loops mechanism in 47% trajectories, and the mixture of single- and two-loop processes is observed in the remaining trajectories. We find that S_k is larger than S_f both for the monomers and dimers (Table II), and both parameters increase as T changes from 0.3 to $0.45 \text{ } \epsilon/k_B$ while the probability to misfolding goes down significantly. In both subcases ("chain A (B present)" and "dimer" in Table II) of the dimeric systems, S_{mf} actually disappears, indicating that the effective crowding environment helps in tying the knots in the individual chains. This behavior is due to the fact that, the effectively crowded environment limits the movement of chains, and thus reduces the entropy of the system. We observe that knots tying temporarily during folding are often different than the native one. Among these, the figure-eight knot is the most popular. It arises from an improper order in which the native contacts form (see Fig. S4 in SM). Backtracking events are necessary to fold the protein correctly⁶⁰. These events are more likely to occur at $T = 0.45 \text{ } \epsilon/k_B$ compared to at $T = 0.3 \text{ } \epsilon/k_B$. Consequently, the misfolding rate S_{mf} of 2EFV at $T = 0.3 \text{ } \epsilon/k_B$ is much higher than that at $T = 0.45 \text{ } \epsilon/k_B$.

We now consider stretching at $T = 0.3 \text{ } \epsilon/k_B$. In the case of the monomeric 2EFV, and of all other monomeric systems, we stretch by N and C. We terminate stretching when the knot is tightened maximally or if the measured force, F , is larger than

10 $\epsilon/\text{\AA}$. Table IV shows the possible final locations of the knot ends. The tightest trefoil knot of 2EFV has 10 residues, which agrees with the finding of ref.¹⁰. The tightened 2EFV knot contains an entire α -helix, such as the cases of {23, 32}, {40, 49}, and {62, 71} shown in Table IV. It may also encompass two different secondary structures, as for location {56,65}. In this case, residue 56 belongs to a β sheet and 65 belongs to an α helix. We also observe the transient location {19,31} in which one knot end is within a helix and another within a turn. Among all possible locations of the tightest knot, {40,49} is the most likely – it minimizes the walking distance from the native location of the knot.

For the homodimeric 2EFV (Fig. 5) there are only four distinct choices of the direction of stretching: N–N', N–C', C–C' and N–C. The first three of these involve the two chains in a direct way. In this case, the protein first ruptures near the stretched termini, then rotates so that the dimeric interface becomes perpendicular to the direction of stretching, and finally the two monomers get separated.¹⁵

The force F , Δn and Q_{INT} as a function of time t are shown in Fig. 8. The figure also shows examples of the corresponding snapshots. Several force peaks in the $F-t$ curve are observed in all schemes; they are labelled by consecutive numbers in the figure. They are all due to the tensile strain¹⁵ – 2EFV has no contacting parallel (or antiparallel) β -strands or α -helices to generate shear mechanical clamps. The last force peak is always due to the separation of the two chains. In scheme N–N', peak 1 of 1.9 $\epsilon/\text{\AA}$ is due to a tensile rupture of 6 contacts (23–58, 26–56, 26–57, 26–58, 27–58, and 27–59) between the backbone knot-loop and the N-terminal domain of chain A. The N-terminal segment gets extended at this force peak. Peak 2 of 1.7 $\epsilon/\text{\AA}$ is due to the rupture of another group of six contacts (31–64, 31–67, 33–70, 33–71, 34–67 and 34–70) between the knot-loop and the N-terminal domain of chain A. At this stage, the knot on chain A gets tightened. The final peak has a height of 0.8 $\epsilon/\text{\AA}$. A similar pattern is observed for scheme N–C'. In scheme C–C', one chain gets untied and another remains knotted. In the bottom left panel of Fig. 8, it is chain B that gets untied. In this case, the first peak of 2.2 $\epsilon/\text{\AA}$ corresponds to dragging of the C-terminus of chain B through its knot-loop in the process of the knot dissolution. The second (and final) peak has a height of 1.5 $\epsilon/\text{\AA}$, and is due to the separation of the two chains.

The tensile force in schemes N–N', N–C' and C–C' results either in the knot tightening (see Δn of schemes N–N' and N–C' in Fig. 8) or in knot untying (see Δn of scheme C–C' in Fig. 8) in single chains. Knot untying shows as Δn becoming equal to the chain length of 82 (without counting the first 5 missing residues). After the separation, both monomers relax and the unknotted chains can fold back to the knotted conformation or misfold, whereas the knotted chains either untie and fold back or make the knot expand and move to another position. Untying of the knot is common. This happens in 82%, 100% and 98% trajectories in schemes N–N' and N–C' and C–C', respectively. Our data shows that the untied monomers separated in schemes N–N', N–C' and C–C' fold back correctly with the probabilities of 17%, 26% and 24% respectively.

In scheme N–C, the knot on the stretched monomer gets tightened while the knot on the other monomer may untie temporarily through the action of the interfacial contacts (see Fig. 8). The simulation ends when chain A is tightened maximally or if the force exceeds 10 $\epsilon/\text{\AA}$ (this criterion also applies to the other dimeric knotted proteins). The two peaks of 1.6 and 1.3 $\epsilon/\text{\AA}$ located at 10.0 and 22.2 /1000 τ respectively (see the bottom right panel of Fig. 8) are due to the tensile rupture of the two groups of contacts between the backbone knot-loop and the N-terminal domain as discussed in the context of scheme N–N'. These processes result in tightening of the chain-A knot. The final locations of the tightened knot are shifted compared to the locations found for the monomeric 2EFV. For instance, the most likely final location of monomeric 2EFV is {40,49}, whereas in the dimeric context it is {44,53}. The location {44,53} is not observed when stretching monomers.

B. 1J85

Folding of the deeply knotted and monomeric 1J85 has been shown to be difficult even in structure-based models and if it happens, then it proceeds through a slipknot conformation^{25,61}. Folding is facilitated by nascent conditions and by inclusion of certain contacts which should count as native²⁶. We expect that folding the dimer is even harder and we do not attempt to study it here.

We now focus on stretching. Table IV shows the locations of knot ends of monomeric 1J85 under stretching. The tightest knot of 1J85 contains 10 residues¹⁰ – as many as in 2EFV. The ends of the tightest knots are located at the sharp turns that are seen in the native structure. For example, location {84,93} contains an entire 3/10 helix, and {94,103} includes an entire β sheet– β 5 (see Fig. S5 in SM). The knot ends can also be stuck in different secondary structures such as in the case of {69,78} and {78,87}. Here, the site 69 is inside an α , 78 is in a β sheet, while 87 is in an 3/10 helix. The most probable location is {78,87}. In this case, the N-terminal end of the knot stays at its native position, while the C-terminal end slides from 119 to 87. Unlike 2EFV, we observe no metastable locations for 1J85. This may be related to the fact that in 2EFV, the native extension of the knot is 63

sites which is substantially longer than 42 sites in 1J85.

Again, there are four possible stretching schemes and the corresponding time dependencies of F are shown in Fig. 9. For schemes N–N', N–C', and C–C', the maximum unravelling force, F_{\max} , is found to be 2.5, 2.4 and 2.3 $\epsilon/\text{\AA}$ respectively. The unfolding mechanism is similar to that of 2EFV. The process consists of three steps and the separation takes place through a tensile action. The separation involves 91 interfacial contacts. The difference is that we observe no untying phenomena and shear forces are involved in the first stages of stretching.

The N–C stretching is very similar to the monomeric case: the most likely locations of the tightened knot are the same, but they come with different probabilities (see Table IV). However, the least likely location of $\{69,78\}$ switches to $\{103,112\}$. The process does not affect the location of the knot in the other chain since all 91 interfacial contacts do not involve the residues in the native knotting core (see Fig. S6 in SM). In the $F - t$ curve of scheme N–C, peak 1 of 1.4 $\epsilon/\text{\AA}$ results from shear between $\beta 1$, $\beta 2$ and $\beta 5$. Peak 2 is due to shear between $\alpha 1$ and $\alpha 5$, and peak 3 due to shear between $\beta 5$, $\beta 4$ and $\beta 6$ of chain A. The conformation of chain B does not change much.

In scheme N–N', peak 1 is due to shear between the parallel β -sheets $\beta 1$, $\beta 2$ and $\beta 5$ (see Fig. S5 in SM) of chain B, while peak 2 is due to shear between $\beta 5$, $\beta 4$ and $\beta 6$ in the same chain. Chain A unfolds after chain B. Peak 3 is due to shear between $\beta 1$, $\beta 2$ and $\beta 5$ of chain A, and peak 4 between $\beta 5$, $\beta 4$ and $\beta 6$. In scheme N–C', the peaks 1 and 3 are due to sheared $\beta 1$, $\beta 2$ and $\beta 5$ in chain A and then $\beta 5$, $\beta 4$ and $\beta 6$ in the same chain. Peak 2 is due to shear between $\alpha 1$ and $\alpha 5$ in chain B. For scheme C–C', the two close peaks in the $F - t$ curve result from shear between $\alpha 1$ and $\alpha 5$ of chain A (first peak) and B (second peak).

C. 2O9C

Protein 2O9C contains a deep figure-eight knot. The crystal structure of the dimerized complex 2O9C⁴⁰ indicates existence of 51 interfacial contacts. Each chain has 322 residues (the first three of them are not provided in the PDB file). The knot ends are located at residues 30 and 271 so the length of the knotting core is 242. The core contains a covalently bound ligand LBV (see Fig. 5). The C3² carbon of LBV is bound to the 24th residue of 2O9C.

We first consider folding of the monomeric system – a process that appears not to be studied experimentally. Fig. 10 shows that the attachment of the ligand generally does not affect the success in folding except that at the optimal temperature of 0.3 ϵ/k_B : the ligand boosts the effectiveness of the process from 10.5 to 13%. In all successfully folded trajectories at the optimal T , folding proceeds by first making the knot and then by establishing the native contacts. This is similar to what is observed in simulations for 1J85 but only at unrealistically high T s⁶². Examples of the folding procedure of holo and apo 2O9C at the optimal folding T are shown in Fig. S7 in SM. The success in proper folding for 2O9C is higher than for 1J85 but lower than for 2EFV. This may reflect the fact that the knot in 2O9C is shallower than in 1J85 but deeper than in 2EFV. We did not succeed in generating folding trajectories for the dimeric 2O9C, which is consistent with the dimer forming in the solution from two folded chains.

Experimental stretching of the 2O9C monomer⁹ has been performed along the direction set by sites 18 and 314, at a constant speed of 1 $\mu\text{m/s}$. The knot was shown to contract to 17 ± 3 residues, as obtained by measuring the countour-length of the protein. It has also been found that there is a significant difference in the unfolding forces between the holo (with the ligand) and apo (without the ligand) forms. The apoprotein unfolds at a force of around 47 pN, while the holoprotein unfolds at 73 pN. The higher forces in the case of holo-2O9C are needed to unfold the ligand that is buried within the protein. The locations of the knot ends of the monomeric 2O9C under mechanical stretching is shown in Table IV both for the holo and apo forms. The presence of the ligand is seen to limit the movement of the knot ends of 2O9C. In case of holoprotein, the location of the knot ends only has three possibilities: $\{44, 122\}$, $\{100, 122\}$ and $\{175, 187\}$, and only 10% of the trajectories are stretched to the tightest knot encompassing 13 residues (see $\{175, 187\}$). For apoprotein, four more possible locations of the knot ends are observed and 72% of them are tightened maximally (as for $\{175, 187\}$ and $\{192, 204\}$). This indicates that a smaller force is needed to stretch apo 2O9C to arrive at the maximally tightened knot than holo 2O9C, which is consistent the experimental observations⁹. However, the span of 13 residues in the tightened knot is smaller than that of 17 ± 3 derived experimentally. This difference either reflects the coarse-grained character of our model, which makes the effective size of a residue to be smaller than in an all-atom description, or – more likely – that the experiment did not go to sufficiently large forces.

For the dimeric 2O9C, we only consider the holo form. In the case of scheme N–C, the knot ends on chain N'–C' essentially do not move, while the knot on chain N–C tightens in steps but never acquires the maximally tightened shape observed in the monomeric simulations (see Table IV). The first force peak of 2.3 $\epsilon/\text{\AA}$ is due to shear involved in stretching the ligand of chain

N–C out of its pocket. The second peak of $3.1 \text{ e}/\text{\AA}$ is arises from shear between three paralleled β sheets (shown in purple in Fig. S5 in SM), and it is stabilized by the immobilization of two regions in the knot-loop of chain A (Fig. S5 in SM, the segments in blue and green) in the process of knot tightening.

In schemes N–N', N–C' and C–C' the monomers get separated through the tensile clamp (see Fig. 11), similar to what happens in the dimeric 1J85 and 2EFV. The force peaks are either due to shear in the interdomain contacts or due to tensile forces. In scheme N–N', peak 1 of $3.4 \text{ e}/\text{\AA}$ is due to the ligand-related shear. Peak 2 of $2.0 \text{ e}/\text{\AA}$ is due to shear between three paralleled α helices (as shown in Fig. S5 in SM and marked in orange). Peak 3 of $1.7 \text{ e}/\text{\AA}$ due to shear between three paralleled β sheets (green), while peak 4 of $1.3 \text{ e}/\text{\AA}$ arises from shear between two β sheets 271 to 279 (pink) and 282 to 291 (green) of chain B. In scheme N–C' there is only one peak. Its height is $2.5 \text{ e}/\text{\AA}$. It arises from shear involved in stretching the ligand of chain A out of its pocket. The tensile peaks associated with the separation of the two chains in schemes N–N' and N–C' are hard to notice, because they almost coincide with the preceding shear-based peak. In scheme C–C', the peak of $1.3 \text{ e}/\text{\AA}$ is due to the tensile forces of separation.

V. CONCLUSIONS

In this paper, we have proposed a pulling-based method to define structural entanglements. Unlike the standard stretching, the method involves all four termini of the two chains that are tested. When making surveys of multi-meric protein structures, we have identified two types of entanglements. In type-II entanglement, there is no chain separation regardless of the direction of pulling and a necessary condition for this situation is that the Gaussian linking number is not smaller than 1. In type I, for which L_k is not larger than 1, the entanglement may or may not show, depending of how one pulls. The entanglements may play various roles and one of them is an enhancement in the thermal stability of the complex.

We have also considered folding and stretching properties of three homodimers 2EFV, 1J85 and 2O9C, which previously have been studied only as single chains. We find that the equilibrium fluctuations RMSF of one chain in the presence of its companion are similar to those of the single chain (see Fig. S8 in SM), except for the region 122–130 in 1J85 where RMSF is suppressed. In spite of this, the presence of the other monomer may result in an enhancement in the success of knotted folding. Folding to the knotted state depends on the temperature at which it is studied but the optimal folding T does not depend on whether one studies the dimeric or the corresponding monomeric system. We find that, for monomers, the ease of folding decreases with the depth of the native knot: the monomeric 2O9C folds easier than the monomeric 1J85. We have also shown that the presence of the LBV ligand in 2O9C slightly enhances the probability of a successful folding (see Fig. 10).

Stretching of the dimers proceeds similarly to that of the corresponding monomers except that there is a tensile-based separation when two chains are involved. If one chain is involved, the presence of the other chain may affect the probabilities of acquiring the final location of the tightened knot. It appears that the experimental studies of stretching of 2O9C⁹ did not probe sufficiently large forces to achieve the ultimate tightening of the knot. The shallowly knotted 2EFV has a rich spectrum of possible behaviors not only during folding but also in stretching. In the monomeric case, the knot in 2EFV can only get tighter. However, in the dimeric case, it may unravel in one chain but not in the other. If it unravels, it may tie back after the separation. Such a variety is not observed in 1J85 and 2O9C.

Supplementary Material. The supplementary material (SM) contains a full list of entangled protein chains that were studied. The SM also provides additional figures. They show: examples of the native and stretched conformations corresponding to type I and type II entanglements; the transient figure-eight knot that arises during folding of 2EFV; a schematic representation of protein 1J85, the crystal structure of protein 2O9C; the interfacial contacts and the RMSF for 2EFV, 1J85, and 2O9C; examples of folding pathways for holo- and apo-2O9C.

Acknowledgments This work has been supported by the National Science Center in Poland under the aegis of the EU Joint Programme in Neurodegenerative Diseases (JPND); grant number 2014/15/Z/NZ1/00037. The local computer resources were supported by the PL-GRID network and financed by the European Regional Development Fund under the Operational Programme Innovative Economy NanoFun POIG.02.02.00-00-025/09.

* Electronic address: mc@ifpan.edu.pl

¹ P. Virnau, L.A. Mirny and M. Kardar, PLoS Comp. Biol. **2**(9), e122 (2006).

² P. Virnau, A. Mallam and S. Jackson, J. Phys. Cond. Mat. **23**(3), 033101 (2011).

³ J. I. Sulkowska, E. J. Rawdon, K. C. Millett, J. N. Onuchic and A. Stasiak, Proc. Natl. Acad. Sci. USA **109**(26), E1715-E1723 (2012).

- 4 J. S. Richardson, *Nature* **268**, 495-500 (1977).
- 5 M. L. Mansfield, *Nat. Struct. Mol. Biol.* **1**(4), 213-214 (1994).
- 6 M. Jamroz, W. Niemyska, E. J. Rawdon, A. Stasiak, K. C. Millett, P. Sułkowski and J. I. Sułkowska, *Nucl. Acid. Res.* **43**, D306-314 (2015).
- 7 K. Koniaris and M. Muthukumar, *Phys. Rev. Lett.* **66**(17), 2211-2214 (1991).
- 8 W. R. Taylor, *Nature* **406**(6798), 916-919 (2000).
- 9 T. Bornschlöggl, D. M. Anstrom, E. Mey, J. Dzubiella, M. Rief and K. T. Forest, *Biophys. J.* **96**(4), 1508-1514 (2009).
- 10 J.I. Sułkowska, P. Sułkowski, P. Szymczak and M. Cieplak, *Phys. Rev. Lett.* **100**(5), 058106 (2008).
- 11 J. Dzubiella, *Biophys. J.* **96**(3), 831-839 (2009).
- 12 M. Chwastyk and M. Cieplak, *Israel J. Chem.* **54**, 1241-1249 (2014).
- 13 K. Lim, H. Zhang, A. Tempczyk, W. Krajewski, N. Bonander, J. Toedt, A. Howard, E. Eisenstein and O. Herzberg, *Proteins* **51**(1), 56-67 (2003).
- 14 O. Nureki, M. Shirouzu, K. Hashimoto, R. Ishitani, T. Terada, M. Tamakoshi, T. Oshima, M. Chijimatsu, K. Takio, D. G. Vassylyev, T. Shibata, Y. Inoue, S. Kuramitsu and S. Yokoyama, *Acta Crystall. D* **58**(7), 1129-1137 (2002).
- 15 M. Sikora and M. Cieplak, *Proteins: Structure, Function, and Bioinformatics* **79**(6), 1786-1799 (2011).
- 16 M. Sikora and M. Cieplak, *Phys. Rev. Lett.* **109**(20), 208101 (2012).
- 17 B. Różycki, Ł. Mioduszewski and M. Cieplak, *Proteins: Structure, Function, and Bioinformatics* **82**(11), 3144-3153 (2014).
- 18 M. Wojciechowski, D. Thompson and M. Cieplak, *J. Chem. Phys.* **141**(24), 245103 (2014).
- 19 M. Cieplak and T. X. Hoang, *Biophys. J.* **84**(1), 475-488 (2003).
- 20 J. I. Sułkowska and M. Cieplak, *J. Phys.: Cond. Mat.* **19**(28), 283201 (2007).
- 21 J. I. Sułkowska and M. Cieplak, *Biophys. J.* **95**(7), 3174-3191 (2008).
- 22 M. Sikora, J. I. Sułkowska and M. Cieplak, *PLoS Comp. Biol.* **5**(10), e1000547 (2009).
- 23 H. Zhang and S. E. Jackson, *Biophys. J.* **111**(12), 2587-2599 (2016).
- 24 F. I. Andersson, D. G. Pina, A. L. Mallam, G. Blaser and S. E. Jackson, *FEBS J.* **276**(9), 2625-2635 (2009).
- 25 J. I. Sułkowska, P. Sułkowski and J. N. Onuchic, *Proc. Natl. Acad. Sci. USA* **106**(9), 3119-3124 (2009).
- 26 M. Chwastyk and M. Cieplak, *J. Phys.: Cond. Matter* **27**(35), 354105 (2015).
- 27 S. a Beccara, T. Skrbic, R. Covino, C. Micheletti and P. Faccioli, *PLoS Comp. Biol.* **9**(3), e1003002 (2013).
- 28 J. K. Noel, J. N. Onuchic and J. I. Sułkowska, *Phys. Chem. Lett.* **4**(21), 3570-3573 (2013).
- 29 M. Chwastyk and M. Cieplak, *J. Chem. Phys.* **143**, 045101 (2015).
- 30 T. C. B. McLeish, *Adv. Phys.* **51**(6), 1379-1527 (2002).
- 31 R. Everaers, S. K. Sukumaran, G. S. Grest, C. Svaneborg, A. Sivasubramanian and K. Kremer, *Science* **303**(5659), 823-826 (2004).
- 32 M. Baiesi, E. Orlandini, A. Trovato and F. Seno, *Sci. Rep.* **6**, 33872 (2016).
- 33 M. Ostermeier and S. J. Benkovic, *Adv. Protein Chem.* **55**, 29-77 (2001).
- 34 M. Jaskólski, *Acta Biochem. Polonica* **48**, 807-828 (2001).
- 35 G. Buck and J. Simon, *Proc. Roy. Soc. A* **468**, 4024-4040 (2012).
- 36 N. Go, *Annu. Rev. Biophys. Bioeng.* **12**(1), 183-210 (1983).
- 37 J. Tsai, R. Taylor, C. Chothia and M. Gerstein, *J. Mol. Biol.* **290**(1), 253-266 (1999).
- 38 G. Settanni, T. X. Hoang, C. Micheletti and A. Maritan, *Biophys. J.* **83**(6), 3533-3541 (2002).
- 39 A. B. Poma, M. Chwastyk and M. Cieplak, *J. Phys. Chem. B* **119**(36), 12028-12041 (2015).
- 40 J. R. Wagner, J. Zhang, J. S. Brunzelle, R. D. Vierstra and K. T. Forest, *J. Biol. Chem.* **282**(16), 12298-12309 (2007).
- 41 N. J. Marianayagam, M. Sunde and J. M. Matthews, *Trends Biochem. Sci.* **29**(11), 618-625 (2004).
- 42 D. S. Goodsell and A. J. Olson, *Ann. Rev. Biophys. Biomol. Syruct.* **29**(1), 105-153 (2000).
- 43 C. Ren, S. Nagao, M. Yamanaka, H. Komori, Y. Shomura, Y. Higuchi and S. Hirota, *Mol. BioSystems* **11**(12), 3218-3221 (2015).
- 44 The data of large structures is usually split over multiple compatible pdb files, which are combined into single bundles.
- 45 C. Schlenker, A. Goel, B. P. Tripet, S. Menon, T. Willi, M. Dlakic, M. J. Young, C. M. Lawrence and V. Copie, *Biochemistry*, **51**(13), 2899-2910 (2012).
- 46 The PyMOL Molecular Graphics System, Version 1.8 Schrodinger, LLC.
- 47 K. Wolek and M. Cieplak, *J. Chem. Phys.* **144**(18), 185102 (2016).
- 48 E. Yamashita, A. Nakagawa, J. Takahashi, K. I. Tsunoda, S. Yamada and S. Takeda, *Acta Cryst. F: Struct. Biol. Cryst. Comm.* **67**(8), 837-841 (2011).
- 49 D. W. Borhani, D. P. Rogers, J. A. Engler and C. G. Brouillette, *Proc. Natl. Acad. Sci.* **94**(23), 12291-12296 (1997).
- 50 B. A. Wallace and K. Ravikumar, *Science* **241**(4862), 182 (1988).
- 51 M. Persson, K. Tars and L. Liljas, *Acta Cryst. D: Biol. Cryst.* **69**(3), 367-372 (2013).
- 52 K. E. Flick, M. S. Jurica, R. J. Monnat Jr and B. L. Stoddard, *Nature* **394**, 96-101 (1998).
- 53 F. G. Whitby and G. N. Phillips, *Proteins: Structure, Function, and Bioinformatics* **38**(1), 49-59 (2000).
- 54 L. D. Cabrita, C. M. Dobson and J. Christodoulou, *Curr. Op. Struct. Biol.* **20**(1), 33-45 (2010).
- 55 C. M. Kaiser, D. H. Goldman, J. D. Chodera, I. Tinoco Jr and C. Bustamante, *Science* **334**(6063), 1723-1727 (2011).
- 56 S. Melnikov, A. Ben-Shem, N. G. de Loubresse, L. Jenner, G. Yusupova and M. Yusupov, *Nat. Struct. Mol. Biol.* **19**(6), 560-567 (2012).
- 57 N. G. de Loubresse, I. Prokhorova, W. Holtkamp, M. V. Rodnina, G. Yusupova and M. Yusupov, *Nature* **513**(7519), 517-522 (2014).
- 58 J. D. Puglisi, *Science* **348**(6233), 399-400 (2015).
- 59 A. H. Elcock, *PLoS Comp. Biol.* **2**(7), e98 (2006).
- 60 J. I. Sułkowska, P. Sułkowski, P. Szymczak and M. Cieplak, *Proc. Natl. Acad. Sci. USA* **105**(50), 19714-19719 (2008).
- 61 W. Li, T. Terakawa, W. Wang and S. Takada, *Proc. Natl. Acad. Sci. USA* **109**(44), 17789-17794 (2012).
- 62 Y. Zhao, M. Chwastyk and M. Cieplak, *Sci. Rep.* **7**, 39851 (2017).

TABLE I: The information on 15 deeply entangled protein pairs.

| classification | PDB code | list of entangled pairs | structural information |
|-----------------------|----------|--|--|
| HYDROLASE | 1A73 | A-B | X-Ray diffraction, hexameric. Van der Waals contacts, C-terminal tail is domain-swapped. |
| LIPID TRANSPORT | 1AV1 | A-B, A-C, A-D, B-C, B-D, C-D | X-Ray diffraction, tetrameric. Hydrophobic interactions. |
| VIRUS | 4ANG | A-B | X-Ray diffraction, 90 dimers. Domain swapped. |
| TRANSFERASE | 2A68 | A-B, D-E, K-L, N-O, C-D, M-N | X-Ray diffraction, hexameric. Polar and hydrophobic interactions. |
| LYASE | 2A8C | C-E, D-F | X-Ray diffraction, tetrameric. Hydrogen bonds. |
| TRANSCRIPTION | 4A9Z | A-B, C-D, A-C, B-D | X-Ray diffraction, tetrameric. Unpublished results. |
| ELECTRON TRANSPORT | 5AUR | A-C, E-G | X-Ray diffraction, dimeric. Domain swapped. |
| RIBOSOME | 5FCJ | D (bundle1) ⁴⁴ -W (bundle1) N (bundle2)-T (bundle3) E (bundle4)-A (bundle5) | X-Ray diffraction. |
| CONTRACTILE PROTEIN | 1C1G | A-B, C-D | X-Ray diffraction, dimeric. Covalent bonds, coiled coil. |
| DNA BINDING PROTEIN | 2ADL | A-B | NMR, dimeric. Hydrogen bonds, domain-swapped. |
| ANTIBIOTIC | 1C4D | A-B, C-D | X-Ray diffraction, dimeric. Hydrogen bonds, domain-swapped. |
| OXIDOREDUCTASE | 2AHR | A-D, B-C | X-Ray diffraction, decameric. Hydrophobic interaction, salt bridges, domain-swapped. |
| STRUCTURAL PROTEIN | 3A1M | A-B, A-C, B-C, D-E, D-F, E-F, A-D, B-F, C-E | X-Ray diffraction, monomeric. Unpublished results. |
| METAL BINDING PROTEIN | 3AQJ | A-B, A-C, B-C, P-Q, P-R, Q-R | X-Ray diffraction, trimeric. Hydrophobic interaction, domain swapped. |
| VIRAL PROTEIN | 4AAI | A-B | NMR, dimeric. Hydrophobic interaction, domain swapped. |

TABLE II: The folding probability of monomeric 2EFV (labeled as 'chain A (monomer)'), chain A in the presence of chain B (labeled as 'chain A (B present)') and dimer (labeled as 'dimer') at $T = 0.3$ and $0.45 \epsilon/k_B$ is denoted as S_f , while their misfolding rate, the knotting probability, median folding time and median knotting time are denoted as S_{mf} , S_k , t_f and t_k , respectively. The data is obtained based on 500 trajectories for each temperature.

| 2EFV | $T = 0.3 \epsilon/k_B$ | | | | | $T = 0.45 \epsilon/k_B$ | | | | |
|---------------------|------------------------|----------|-------|------------------|------------------|-------------------------|----------|-------|------------------|------------------|
| | S_f | S_{mf} | S_k | t_f (τ) | t_k (τ) | S_f | S_{mf} | S_k | t_f (τ) | t_k (τ) |
| chain A (monomer) | 5% | 72% | 18% | 6186 | 24600 | 65% | 13% | 87% | 8018 | 4000 |
| chain A (B present) | 44±6 % | 6±3% | 60±1% | 5075±1225 | 17375±4575 | 50±15% | 0% | 91±1% | 290850±70625 | 4400 |
| dimer | 3% | 19% | 32% | 12854 | - | 6% | 0% | 83% | 687548 | - |

TABLE III: The probability of folding dimeric 2EFV via three possible pathways .

| pathways | $T = 0.3 \epsilon/k_B$ | $T = 0.45 \epsilon/k_B$ |
|----------------|------------------------|-------------------------|
| \mathbb{F}_1 | 56% | 0% |
| \mathbb{F}_2 | 19% | 3% |
| \mathbb{F}_3 | 25% | 97% |

TABLE IV: The locations of the knot ends of 2EFV, 1J85 and 2O9C under the N-C stretching scheme at $T = 0.3 \epsilon/k_B$.

| Protein | | locations of the knot ends | | | | | |
|---------|---------|----------------------------|----------------|----------------|-----------------|----------------|------------------------|
| 2EFV | monomer | {19,31} 8% | {23,32} 8% | {40,49} 66% | {56,65} 2% | {62,71} 16% | – – |
| | dimer | {44,53} 52% | {38,47} 6% | {40,49} 24% | {56,65} 18% | – – | – – |
| 1J85 | monomer | {69,78} 2% | {78,87} 44% | {84,93} 22% | {94,103} 32% | – – | – – |
| | dimer | {103,112} 6% | {78,87} 24% | {84,93} 34% | {94,103} 36% | – – | – – |
| 2O9C | monomer | {44,122} | {100,122} | {175,187} | {187,200} | {192,204} | {204,248} or {204,284} |
| | holo | 54% | 36% | 10% | – | – | – |
| | apo | 6% | 2% | 66% | 10% | 6% | 10% |
| | dimer | {44,122} | {100,122} | – | – | – | – |
| | holo | 92% | 8% | – | – | – | – |

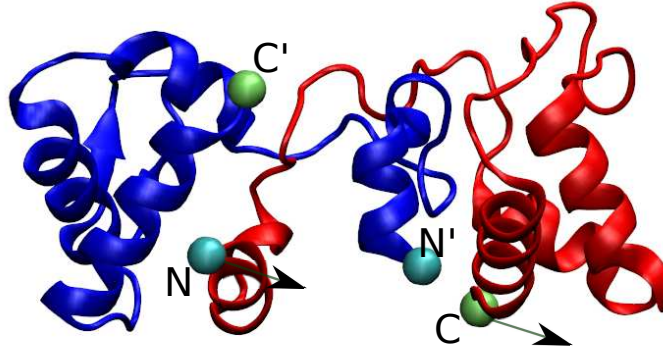


FIG. 1: An example of the direction of stretching for 5AUR. One chain (A) is in red and another (C) in blue. The N and N' termini are marked in cyan and the C and C' termini in lime. The indicated direction of pulling leads to chains A and C being entangled.

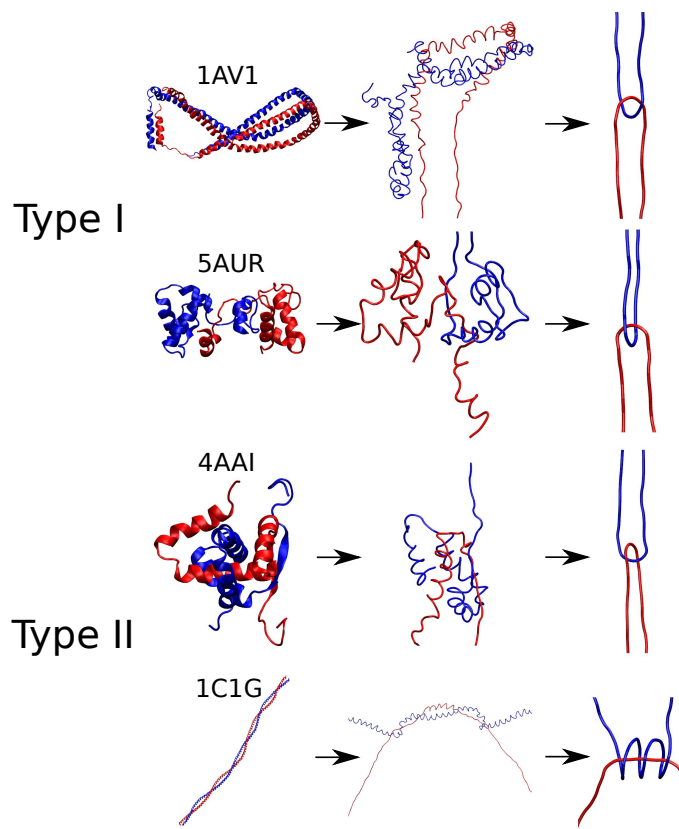


FIG. 2: Stages of pulling at the termini N and C while anchoring N' and C' simultaneously, or vice versa. The top two examples (chains A and B in 1AV1, chains A and C in 5AUR) correspond to entanglement of type I and the remaining (chains A and B in 4AAI and 1C1G) – of type II. The absolute value of L_k of 1AV1, 5AUR, 4AAI and 1C1G is 1, 1, 1 and 3, respectively.

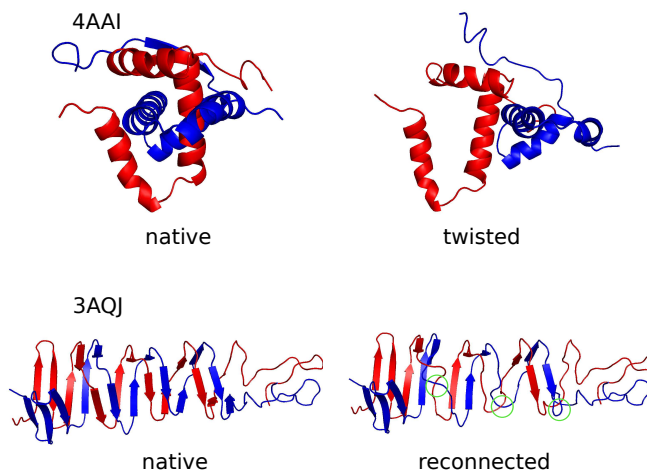


FIG. 3: The native (left) and twisted (right) structures of 4AAI (top), and the native (left) and reconnected (right) structures of 3AQJ (bottom). The green circles show the three sites in 3AQJ where the reconnection is made.

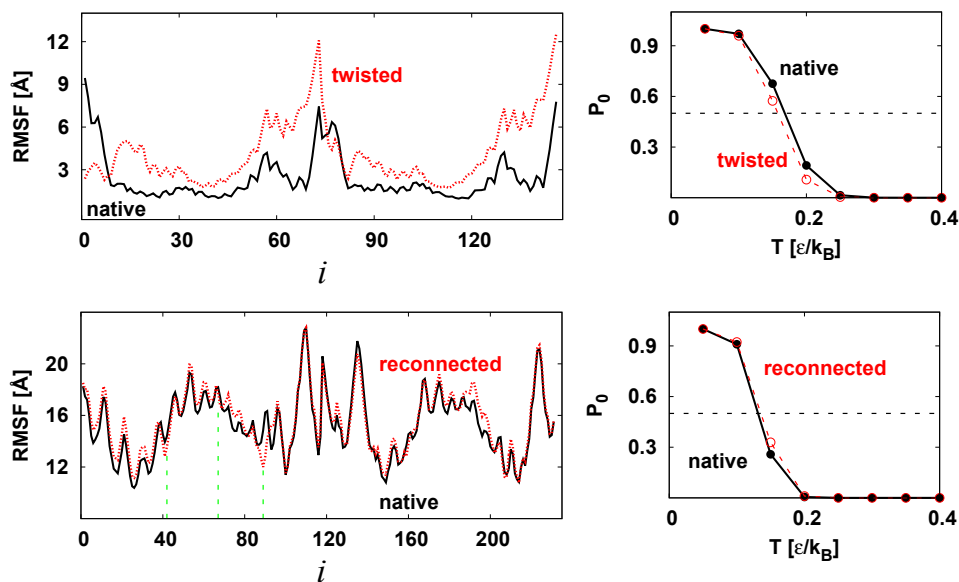


FIG. 4: Comparison of the physical properties corresponding to the two forms of 4AAI (top) and 3AQJ (bottom) shown in Fig. 3. The left panel shows the RMSF at $T = 0.3 \epsilon/k_B$ and the right panel – the T -dependence of P_0 . The T at which P_0 crosses $\frac{1}{2}$ defines the folding temperature. The size of the data points is a measure of the error bars. Chain A (B) of 4AAI ranges from residue 1 to 73 (74 to 146), while chain A (B) of 3AQJ ranges from residue 1 to 117 (118 to 231). The green dash lines indicate the sites in chain A of 3AQJ at which the reconnection was made.

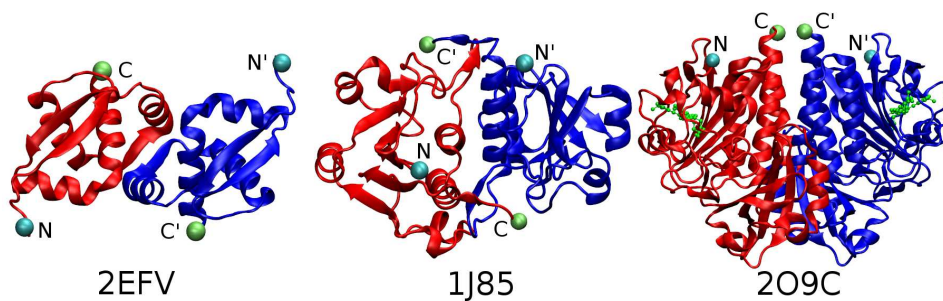


FIG. 5: Structural representations of the proteins studied here 2EFV (left), 1J85 (middle) and 2O9C (right). Monomers A and B of these homodimeric structures are shown in red and blue respectively. The N and N' termini are marked in cyan and the C and C' termini in lime. The ligand of 2O9C is colored in green.

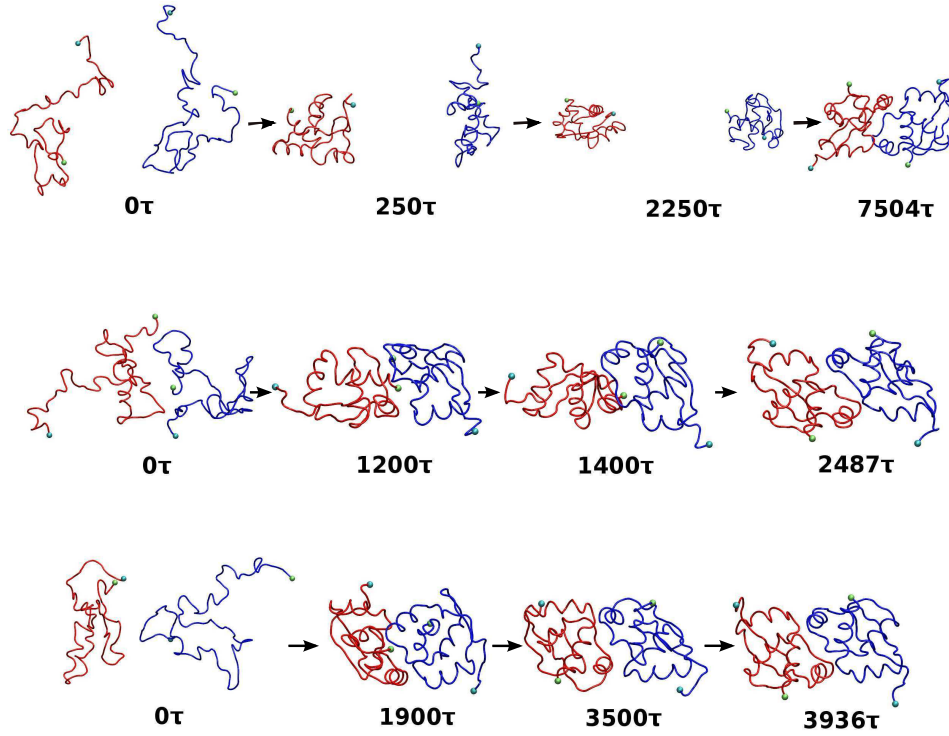


FIG. 6: Examples of folding pathways for the dimeric 2EFV at $T = 0.3 \epsilon/k_B$. For \mathbb{F}_1 (top), the folding order is: monomer B–monomer A–interface. Monomer A of the trajectory is knotted at 6100τ , and monomer B is knotted at 5700τ . In \mathbb{F}_2 (middle), the folding order is: monomer B–interface–monomer A. Monomer A of the trajectory is knotted at 1700τ , and monomer B is knotted at 1300τ . The folding order in pathway \mathbb{F}_3 (bottom) is: interface–monomer B–monomer A. Monomer A of the trajectory is knotted at 3300τ , and monomer B is knotted at 3200τ .

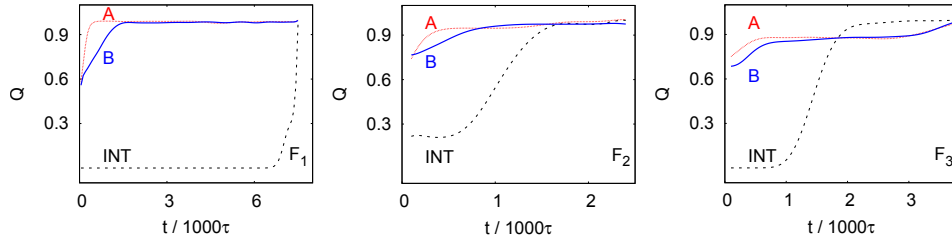


FIG. 7: Time evolution of Q on the folding pathway \mathbb{F}_1 , \mathbb{F}_2 and \mathbb{F}_3 of dimer 2EFV at $T = 0.3 \epsilon/k_B$.

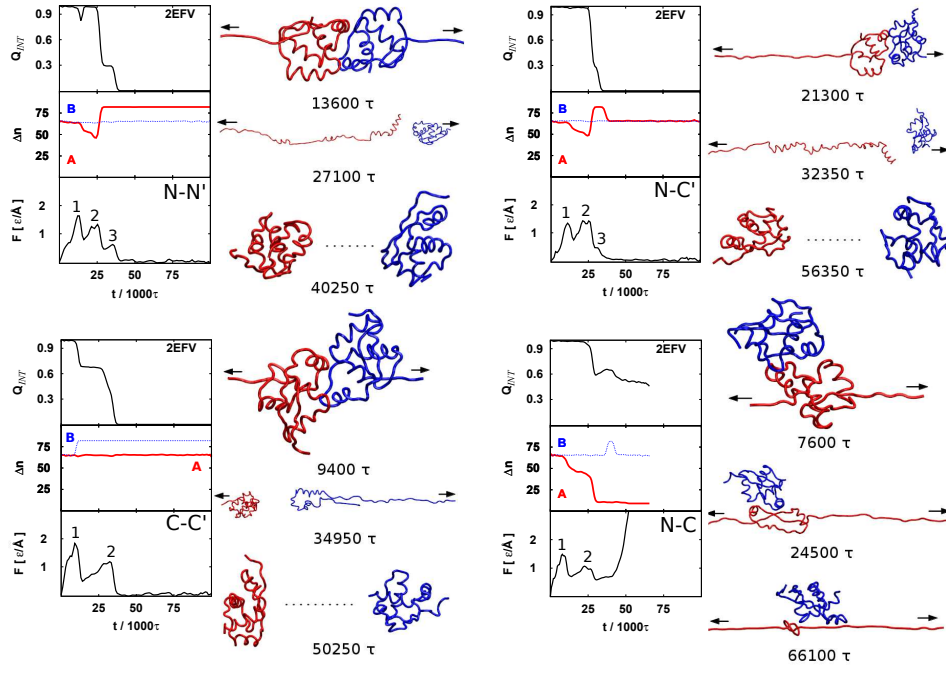


FIG. 8: The time evolution of Q_{INT} , Δn and F for the 2EFV dimer for various schemes of stretching, as indicated. Examples of the conformations seen during stretching (at $T = 0.3 \epsilon/k_B$) are shown to the right of the data panels. Chain A and B are colored in red and blue, respectively.

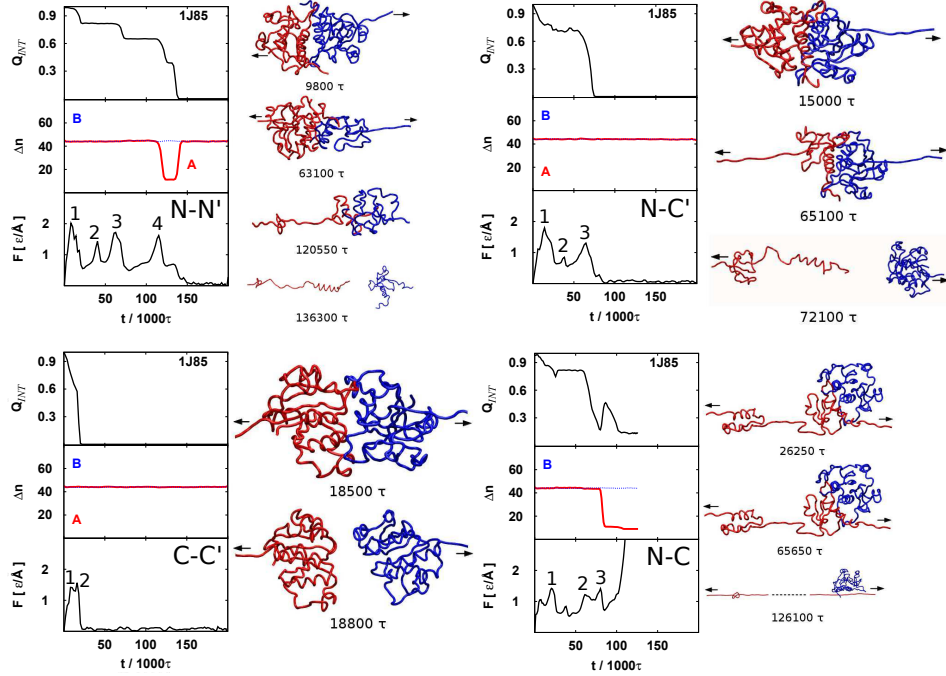


FIG. 9: The time evolution of Q_{INT} , Δn and F for the 1J85 for various schemes of stretching as indicated. Conformations corresponding to characteristic stages of stretching are shown to the right of the data panels. Chain A and B are colored in red and blue, respectively.

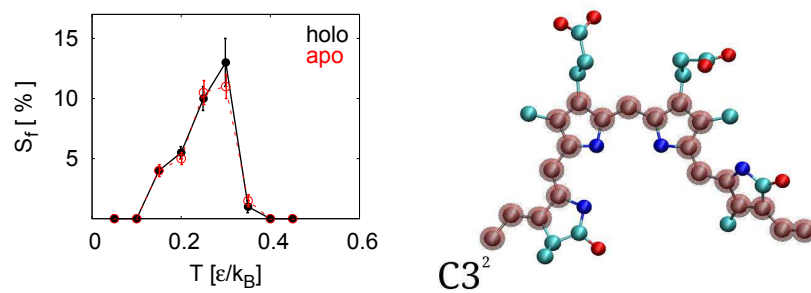


FIG. 10: Left: The success rate of proper folding of monomeric 2O9C in both holo and apo forms as a function of T . Right: Schematic representation of the atomic structure of ligand LBV. The carbons, nitrogens and oxygens of the ligand are displayed as cyan, blue and red beads, the hydrogen atoms are not shown. The red-cyan beads are the backbone carbon atoms of the ligand.

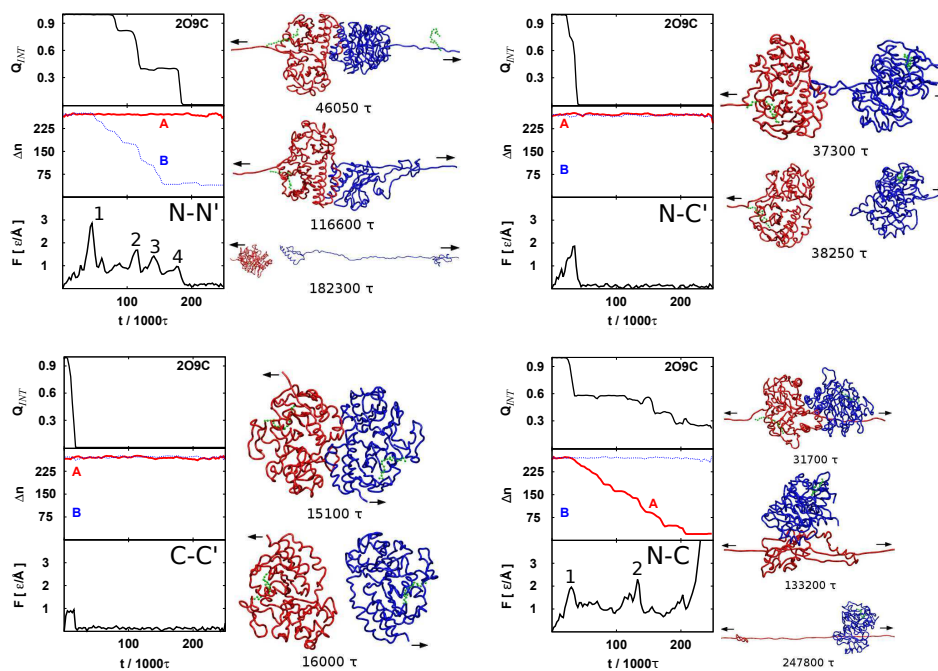


FIG. 11: Similar to Fig. 9 but for the 2O9C dimer. The ligand of 2O9C is colored in green.